Locally and Dynamically Controllable Surface Topography Through the Use of Particle-Enhanced Soft Composites

Mark Guttag and Mary C. Boyce*

A new class of soft composite materials with dynamically tunable and reversible surface topographies is introduced that allows a wide diversity and local positioning of surface features. The particle-enhanced soft composites are comprised of a soft elastomeric matrix with relatively stiff particles embedded below the surface. Upon application of external stimuli, a surface that is originally smooth and flat (or of other initial topology) transforms to engineered surface topographies. Finite element based micromechanical simulations are used to design and study the hybrid material structures that govern the evolution in surface topographies. Physical prototypes are fabricated using multimaterial 3D-printing, and then experimentally evaluated to validate the accuracy of our simulations. It is demonstrated that a rich variety in periodic and random surface features including variable waves, crease-like features, flat apexes, and valleys can be attained by changing different dimensionless geometric parameters (e.g., relative particle size, shapes, spacing, and distributions). Furthermore, these surface features can be locally controlled by positioning of particles and do not rely on instabilities. The material design depends primarily on the geometry of the particles and the arrays, making this approach to on-demand custom and reversible surface patterning applicable over a wide range of size scales.

1. Introduction

The study of surface texture is important in fields including natural camouflage,[1] wetting and nonwetting surfaces,[2] hydrodynamics,[3] biofouling,[4] and many others. For some applications, creating a static surface texture is sufficient, for others (e.g., drag reduction and camouflage) the ability to create a tunable and reversible surface topography provides an advantageous ability to adapt the surface behavior or attribute to the need at hand. Moreover, it is often important to have local control over exactly which features are induced at which location. Natural and statically engineered surface topologies are found to exhibit a rich range in feature geometries from periodic to random bumps, from papilla to ridges to creases to channels, depending on the desired physical or chemical behavior. Methods for creating complex static surface topographies are numerous,[5] but there are no previous techniques that provide comparable flexibility for creating dynamically and locally tunable and reversible surface changes.

One existing method for creating tunable and reversible surface topographies is through the use of surface wrinkling. Recent work has investigated the implementation of wrinkling for adhesive,[6] electrical,[7] optical,[8] and other applications.[9] Periodic sinusoidal-like patterns of parallel wrinkles with a characteristic wavelength and amplitude have been created through axial stressing of a relatively stiff film on compliant substrates;[10,11] more complex wrinkle patterns result from equibiaxial stress states. These patterns include herringbone, hexagonal, labyrinth, and checkerboard waveforms.[12] The patterns attainable through wrinkling are composed of differently organized pockets of sinusoidal wrinkles. The pockets can be uniform lines of sinusoids (like those created via axial compression), zigzags of sinusoids, labyrinths of sinusoids, and so forth. While wrinkled surfaces have many applications, it is difficult to use wrinkling to produce locally controlled surface deformations or topologies that are not inherently some forms of sinusoidal wave pattern.

In contrast to wrinkling, where a stiff material is adhered to the surface of a soft substrate, here we introduce a class of material design where stiff particles are embedded beneath, but near, the surface *inside* a soft substrate to specifically control surface topology. These particle-enhanced soft composites (PESCs) are comprised of an elastomeric matrix with stiff particles embedded below the surface of the matrix in ordered arrays or in random distributions. This material design provides numerous opportunities for achieving different surface topographies by varying various material design parameters. The topographic change is governed by the size, shape, spacing, and arrangement of the particles along with the contrasting material properties of the matrix and the particles. Our proposed method depends primarily on the geometry of the particles and the arrays; hence it can potentially be

M. Guttag
Department of Mechanical Engineering
Massachusetts Institute of Technology
77 Massachusetts Ave. Bldg. 5-426, Cambridge
MA 02139, USA
E-mail: mguttag@mit.edu
Prof. M. C. Boyce
School of Engineering and Applied Sciences
Columbia University
510 S.W. Mudd Building, Mail Code 4714, 500 West 120th Street,
New York, NY 10027, USA

DOI: 10.1002/adfm.201501035

applied to many different length scales and materials, and thus to many applications that would benefit from changing surface topography. Furthermore, the surface transformation can evolve continuously and can also be reversible. This method retains the soft surface, and enables the formation of many locally controllable topographies.

The ability to create locally controllable topographies facilitates many potential applications. For example consider a surface designed to control the path of fluid flow. Imagine a flat surface with a slight tilt. Water would flow off the surface evenly. One could then apply a stress that would cause the surface to transform into one with "streams" that would guide the flow to "ponds" that would capture specific amounts of the fluid in specific places.

2. Results and Discussion

2.1. Computational Approach

Figure 1a shows a representative segment of an exemplar PESC subjected to progressively increasing macroscopic strain (here, through an applied displacement, but the strain could also be achieved with a stimulus-responsive matrix). The gray background indicates soft matrix and the black circles indicate stiff particles. Initially, the upper surface is flat and smooth (however, an initial topography could be an alternate starting point), and the deformation-induced evolution in surface topography is depicted after 5%, 10%, 15%, and 20% strain, showing the ability to tune the surface topography and also the ability to create nonsinusoidal and complex surface features.

The surface topography evolutions shown in Figure 1a, and other figures in this paper, were generated using finite element-based micromechanical simulations that explore hybrid material design attributes that govern the deformation-induced tuning of surface topographies. Additionally, physical prototypes of select material designs were fabricated using multimaterial 3D-printing, and then experimentally tested to validate the accuracy of our simulations. In the simulations, the matrix is taken to be a nearly incompressible neo-Hookean elastic material with shear modulus G = 0.33 MPa, and the particles are taken to be linear elastic with Young's modulus E = 1.5 GPa and Poisson's ratio ν = 0.490—these properties correspond to those of the physical experiments. Details of the simulations and experiments are provided in the methods section at the end of the paper. We focus on 2D material designs, but the material design concept is easily extended to 3D geometries, which further expands the surface topographies possible.

Figure 1b shows a representative volume element of a PESC with a three-row staggered array of particles near a surface, indicating the important geometric features that are used to construct dimensionless parameters that are varied in the simulations to examine their influence on local surface topography. The influence of relative interparticle ligament length $\left(\frac{a-2\beta}{a}\right)$, particle aspect ratio (α/β), number of rows of particles (N), and periodic staggered versus irregular distributions are presented.

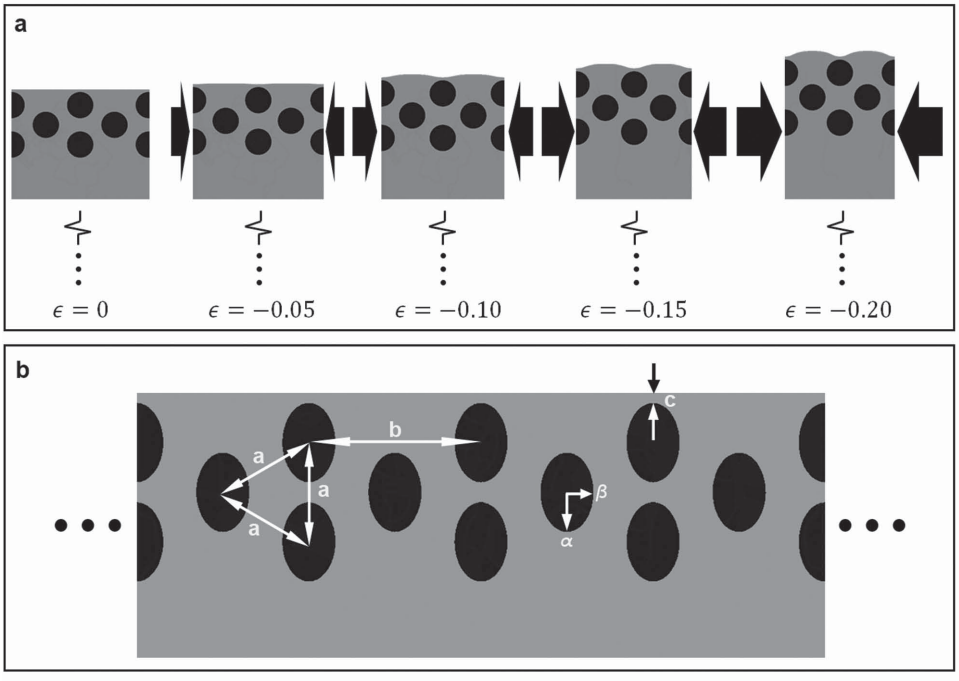

Figure 1. Basic setup of the PESCs. a) The results of finite element simulations of a representative segment of an exemplar PESC at various global compressive strains through applied displacement. The black represents the stiff particles, and the gray represents the soft matrix. b) A representative PESC with important geometric dimensions labeled. Note that $b = a\sqrt{3}$.

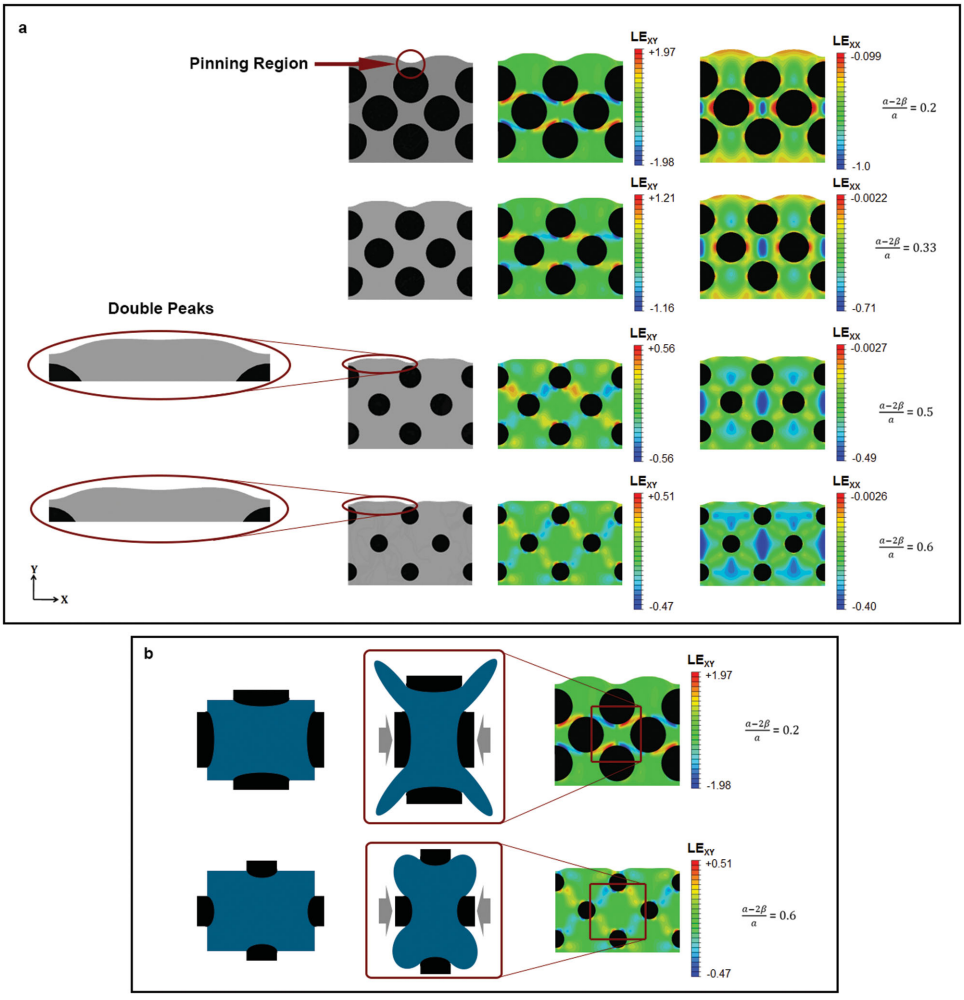

Figure 2. Effect of relative interparticle ligament length $\left(\frac{a-2\beta}{a}\right)$ on surface topography. a) The results of simulations with several different values of $\frac{a-2\beta}{a}$. The first column shows the surface with important features circled, the second column shows the shear strain in the matrix, and the third column shows the axial strain in the matrix. b) A schematic diagram of the extrusion mechanism responsible for the resulting surface topography.

2.2. Micromechanical Simulation Results and Discussion

2.2.1. Relative Interparticle Ligament Length

We first examine relative interparticle ligament length, $\frac{a-2\beta}{a}$ while fixing the particle aspect ratio (α/β=1, i.e., circular particles), the relative distance from the surface $\left(\frac{c^2}{a\times\beta}=0.04\right)$, and the number of rows ($N=3$). The interparticle spacing is $b=a\sqrt{3}$ and hence the relative interparticle spacing is $\frac{b-2\beta}{b}$ or $\frac{a\sqrt{3}-2\beta}{a\sqrt{3}}$. As we will show, the effect of deformation on surface topography depends on the relative length of matrix material between particles which can be expressed either in terms of relative interparticle ligament length or relative interparticle spacing. **Figure 2**a shows results of simulations at 20% global compressive strain for values of $\frac{a-2\beta}{a}$ ranging between 0.2 and 0.6. In general, the surface topography evolves to exhibit multiple local features: a smooth "bump" between two particles in the top row anchored by a "pinning region" at the top of each particle in the first row. In the first row of Figure 2a, for relatively small interparticle spacing (i.e., relatively large particles compared to length of matrix material between particles), between the pinning regions the surface topography has a single large smooth bump. The peak of the bump is aligned directly above the particles in the second row. As $\frac{a-2\beta}{a}$ is increased to 0.33, there is still a single peak aligned directly above the particles in the second row; however, the bump is a bit flatter than with the smaller relative interparticle ligament length. When the relative interparticle ligament length is increased to a $\frac{a-2\beta}{a}$ value of 0.5 or greater, there is no longer a single peak located above the particles in the second row. Instead, what appears is a local minimum aligned at that location. These local minima lead to surface features with "double peaks."

The dependence of the shape of the surface bump on relative interparticle spacing can be understood by examining the mechanics of the deformation in the strain contours of Figure 2a. The second column in the figure is the X–Y shear

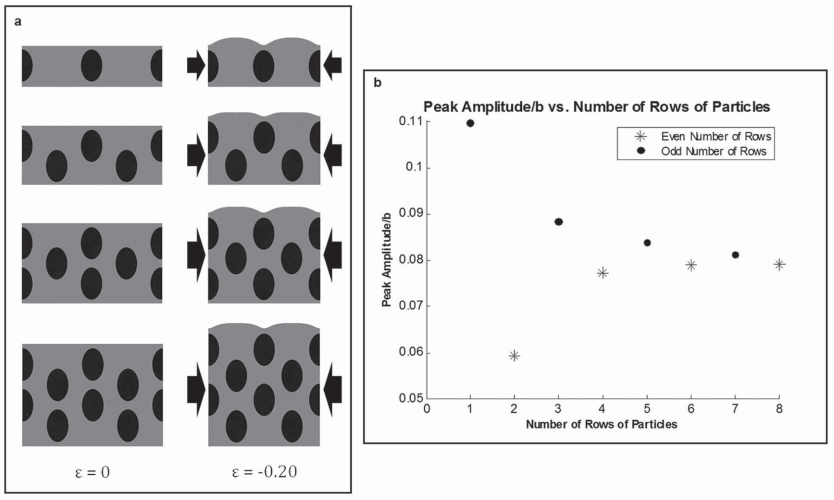

Figure 3. Effect of the number of rows of particles on the surface topography. a) The results of simulations with different rows of particles at 0% and 20% global compressive strain. b) The peak amplitude (defined as the distance between the highest and lowest points on the surface) normalized by the horizontal particle spacing b plotted against the number of rows of particles.

strain and the third column is the X–X normal strain. These contours depict extensive interparticle matrix shearing, which acts to diagonally extrude matrix material up toward the surface creating the surface protrusions shown in Figure 2b. This acts in concert with the lateral compression between particles in the same row, which (because of the near incompressibility of the matrix) results in the longitudinal expansion. For relatively smaller ligaments, this results in a single centric peak because of the intersection of the extrusions from the concentrated interparticle shearing, as seen by the well-defined shear bands for the smaller interparticle spacing. For relatively larger interparticle spacing, the shear is still localized diagonally between the staggered particles, but is focused near the particle edges and the extrusions from neighboring particles do not intersect and hence produce the double peaks between particles. Regions of high stress occur at the particle/matrix interface. In principle, the interfacial stresses could lead to debonding. However, no sign of debonding was observed in any of our experiments likely due to the nature of the particle/matrix interfaces in our 3D printed materials. As in most composite material systems, attention should be provided to the integrity of interfaces between constituents.

2.2.2. Number of Rows of Particles

Multiple rows of particles can be used to achieve surface changes that cannot be achieved with a single row. To investigate the effect of the number of rows of particles on the surface topography we arranged the particles in a hexagonal array similar to that used in investigating the effect of interparticle ligament length. We held constant the relative distance from the surface $\left(\frac{c^2}{a\times\beta}=0.094\right)$, the aspect ratio of the particles ($\alpha/\beta = 1.5$) and the relative interparticle ligament length $\left(\frac{a-2\beta}{a}=0.47\right)$.

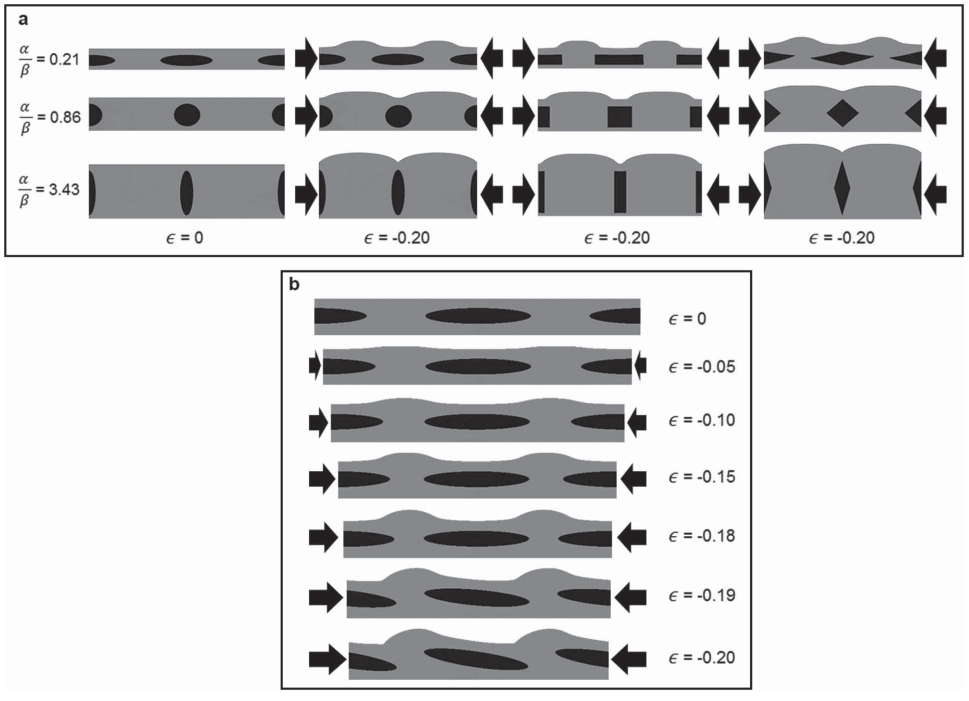

Figure 4. Effect of aspect ratio of the particles on the surface topography. a) The results of simulations with three different particle aspect ratios of ellipsoidal, rectangular and diamond shaped particles. b) The results of the simulation with an aspect ratio of $\alpha/\beta = 0.15$. At a critical compressive strain between 18% and 19% the particles rotate in the matrix.

Figure 3a shows the results of simulations for PESCs with differing numbers of rows of particles at 0% and 20% global compressive strain. In the top row of the figure, in which the PESC has a single row of particles, the surface develops a large bump aligned between adjacent particles in the first row. When a second row of particles is added, the surface assumes a flatter shape, and the bumps have a double peak. When a third row of particles is added, the surface takes a shape that is somewhere between the shapes it made with a single row of particles and two rows of particles. Adding a fourth row of particles produces little change.

The effect of the number of rows of particles was quantified using the peak amplitude, the vertical distance between the highest and lowest points on the surface. Figure 3b shows peak amplitude normalized by the particle spacing plotted against the number of rows of particles. The peak amplitude was largest for a single row of particles and smallest for the PESC with two rows of particles. Each successive odd row of particles that is added causes an increase in peak amplitude and each even row that is added causes a decrease in peak amplitude. However, every time a new row is added it causes the peak amplitude to change by less than the previous row did.

2.2.3. Aspect Ratio of Particles

To investigate the effect of the aspect ratio (α/β) of the particles on the surface topography, PESCs consisting of a single row of particles were studied while holding constant the relative interparticle center-to-center distance $\left(\frac{b^2}{a\times\beta}=64.28\right)$ and the relative distance from the surface $\left(\frac{c^2}{a\times\beta}=0.21\right)$. **Figure 4**a shows simulations in which the aspect ratio of the particles was varied for particles of different shapes. Changing the aspect ratio of the particles dramatically changes the surface topography. For the higher values of α/β (the narrower particles) the pinning regions form sharp valleys while the area between pinning regions form a single wide bump. The pinning regions of the PESCs with lower values of α/β form wider valleys with narrower bumps in between. This happens because the wider particles constrain the deformation of a larger region of the surface.

Figure 4b shows the results of a simulation for a PESC with a wide elliptical particle. Between 18% and 19% global compressive strain the particles rotate in the matrix. This instability causes the surface to suddenly change from a symmetric shape to a nonsymmetric shape. The instability occurs upon reaching a critical strain and demonstrates the ability to create a trigger to give a sudden switch in surface topography from one with a directionally symmetric topology to one with a directionally biased topography.

2.2.4. Nonuniform Arrays of Particles

Figure 5a shows the results of simulations in which the PESC is made up of smaller circular particles embedded in the matrix between larger circular particles. Compared to row 3 of Figure 2a, the addition of the smaller particles causes the double peak to become more pronounced. The valley located above the smaller particles has a larger radius of curvature for the case where the top of both the bigger and smaller particles are initially the same distance from the surface (the first row of the figure) than for the case where the central horizontal axis of the smaller particles is initially aligned with the central horizontal axis of the larger particles (the second row of the figure). When the smaller particles are closer to the surface, those particles more easily constrain the deformation of the matrix causing the pinning region to be larger. The larger pinning region leads to a larger radius of curvature. When the pinning region is smaller, the resultant smaller radius of curvature generates a crease-like feature, as seen in the second row Figure 4a. It is known that uniaxial compression of a semi-infinite elastomer block causes creases to form at random locations at a critical compressive strain of about 35%.[13,14] The use of PESCs could enable the tailored positioning of crease-like features as well as the ability induce them at prescribed strains less than 35%.

Figure 5b shows a PESC with a mixture of particles with different sizes, shapes, and orientations. It illustrates the

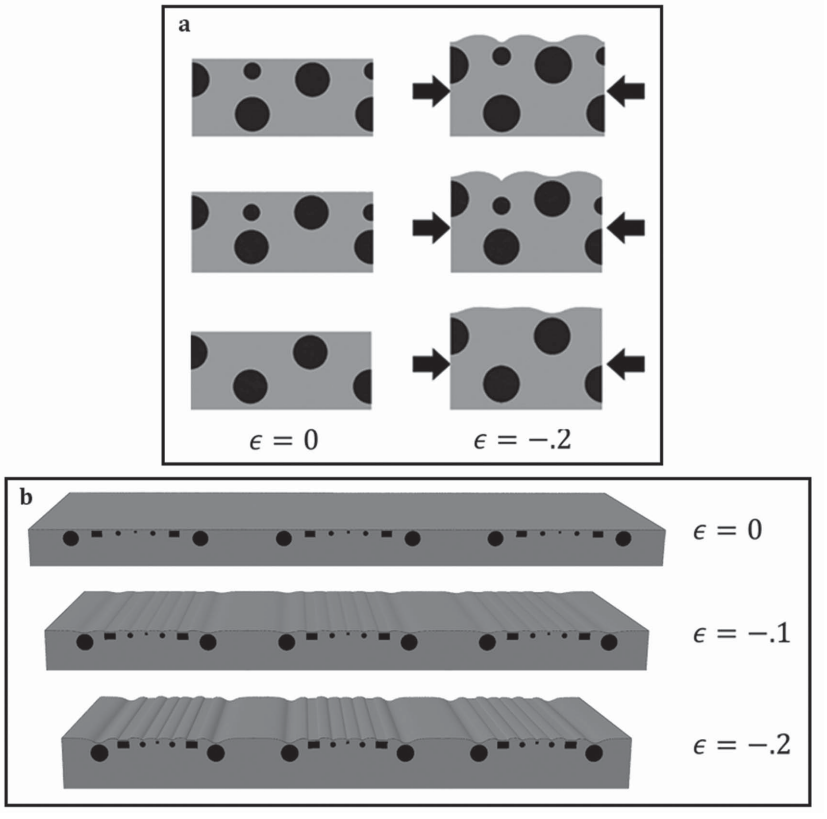

Figure 5. Effect of nonuniform arrays of particles on the surface topography. a) Simulation results of PESCs with smaller particles embedded in the matrix between larger particles. b) Simulation results of a PESC made up of particles with different shapes and sizes shown in perspective to demonstrate the ability to locally control the surface topography.

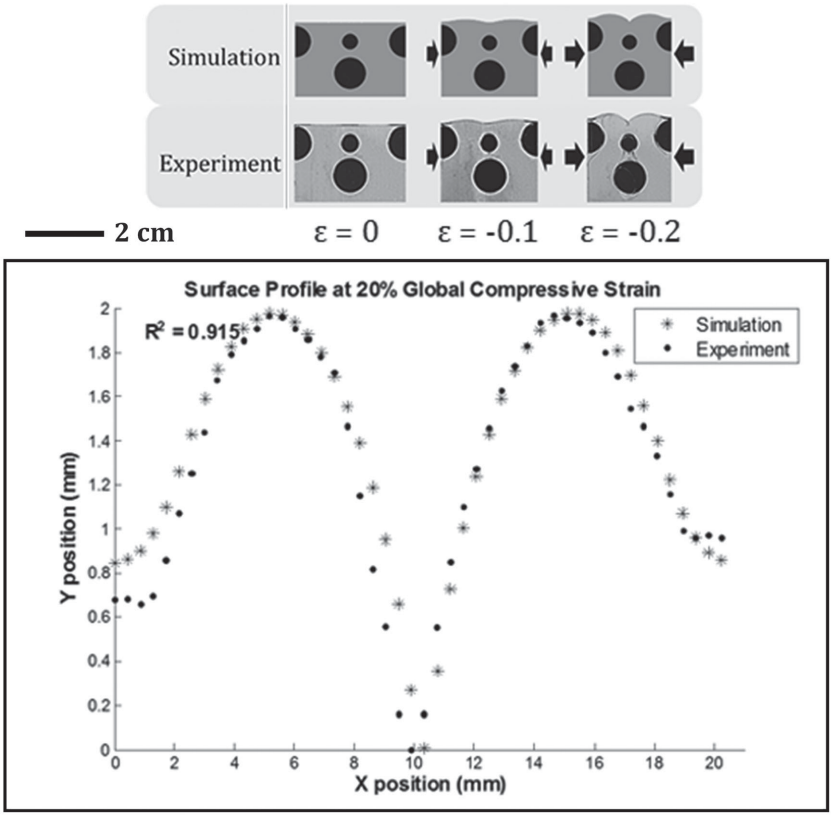

Figure 6. Results of experiments performed to verify the simulations. The top of the figure shows images of a simulation and an experiment at various global compressive strains. The bottom of the figure shows a plot of the surface profile of both the simulation and the experiment. The R^2 value is 0.915 and was the lowest of all the experiments run.

ability to achieve fine-grained local control over surface features. The deformed surface of the PESC shows a variety of different local topographical features generated in a single PESC. In this case, we generated a sequence of wells of different sizes and shapes. Local control is derived from the fact that the shape of each topographical feature is controlled primarily by the particles in the immediate vicinity of the feature. For example, some of the wells have flat bottoms because the pinning particle is rectangular rather than ellipsoidal, and the increased size of some of the wells is caused by the increased particle size.

2.3. Experimental Validation

To validate the simulation results, physical experiments were carried out using 3D-printed samples. The 3D-printed samples were used in compression tests in which the PESC was sandwiched between optically clear acrylic plates (to ensure plane strain conditions), lubricated with mineral oil to reduce friction between the sample and plates, and then compressed to 20% global strain using a Zwick/Roell Z2.5 mechanical tester. Images of the surface were captured with a high resolution camera. It is worth noting that in the experiments no debonding was observed between the matrix and the particles.

Figure 6 shows images of both experimental and simulation results of one PESC arrangement. The images show a single unit cell, the unit cell closest to the compressor head. The plot in the figure shows the surface profile of one simulation and the corresponding experiment. For each of the experimental validations the R^2 values were between 0.90 and 0.99, indicating consistently good agreement between the simulations and experiments.

3. Conclusions

In this paper we showed how particle-enhanced soft composites can be used to create a variety of dynamically tunable and localizable 2D surface topographies. Extending the work to 3D structures would increase the number of useful arrangements of the particles, and the particles themselves could be spheres, ellipsoids, plates, blocks, etc. Extending to 3D also opens the door to a variety of other loading conditions and mechanisms.

In many applications simple compression is a practical method to activate the mechanism. However, there are also a number of other possible activation mechanisms. Any mechanism that causes differential changes in the volumes of the matrix and the particles is potentially suitable. Possible candidates include pH responsive materials and other active materials which respond to electrical and/or thermal stimulation.

The flexibility offered by PESCs provides a new and novel material design for tunable surface topographies that apply to applications across a wide range of length scales. PESCs offer the freedom to adapt the surface topography in order to optimize performance under changing conditions ranging from applications as diverse as light reflection, wettability, friction, adhesion, hydrodynamics, and even transport and propulsion. For example, by dynamically controlling the patterned hydrophobicity of a surface,[15] a liquid could be collected and then transported to a desired location on that surface.

Controlling surfaces with PESCs could be particularly useful for applications in which the environment surrounding the surface is changing in a way that requires local dynamic changes to the surface.

4. Experimental Section

For the physical experiments, the samples were created by an Objet500 Connex Multi-Material 3D Printer. The matrix was made of TangoPlus and the particles were made of VeroBlack (both proprietary

materials available as outputs from the 3D printer). The compressive tests were run with a Zwick/Roell Z2.5 mechanical tester. In order to ensure the experiments were run under plane strain conditions the samples were sandwiched between two optically clear acrylic plates. Each plate had four laser cut holes through which we slid bolts to connect the plates together and tighten them around the sample. Two bolts were placed on each side of the sample with a spacer the same width as the sample. The spacers were positioned directly next to the bolts on either side of the sample. Mineral oil was applied to the surface of the plates and the face of the sample in order to reduce the friction between the plates and the sample. To compress the sample, an acrylic plate slightly narrower than the width of the sample was placed between the top of the sample and a steel plate that was attached to the load cell of the Zwick. Another acrylic plate, the same width as the one above the sample, was placed below the sample, so that the top and bottom boundary conditions were the same. Mineral oil was also applied to the surfaces of the top and bottom acrylic plates to reduce the friction between the acrylic and the sample. The tests were run up to –20% global strain for each sample with a strain rate of 0.00167 s^{-1}.

During the tests a high resolution camera was setup on a tripod in front of the sample, and set to take a picture every half second. The camera was a Point Grey CMLN-13S2M camera with a Nikon AF Micro-Nikkor 60 mm f/2.8D lens. Adobe Photoshop was used in tandem with a custom MATLAB script to extract the surface profiles of the experimental images taken with the camera. The experimental surface profiles were then compared to the simulation surface profiles by calculating the coefficient of determination (R^2).

Acknowledgements

This work was funded by the Cooperative Agreement between the Masdar Institute of Science and Technology (Masdar Institute), Abu Dhabi, UAE and the Massachusetts Institute of Technology (MIT), Cambridge, MA, USA – Reference 02/MI/MI/CP/11/07633/GEN/G/00. Both authors worked on writing the paper, designing experiments, the invention of concept and data analysis. Mark Guttag worked on running experiments and simulations.

Received: March 16, 2015
Revised: April 9, 2015
Published online: May 7, 2015

[1] J. J. Allen, G. R. R. Bell, A. M. Kuziria, R. T. Hanlon, *J. Morphol.* **2013**, *274*, 6.
[2] S. Herminghaus, *Europhys. Lett.* **2000**, *52*, 2.
[3] S. Granick, Y. Zhu, H. Lee, *Nat. Mater.* **2003**, *2*, 4.
[4] H. C. Flemming, *Appl. Microbiol. Biotechnol.* **2002**, *59*, 6.
[5] A. Tuteja, W. Choi, M. L. Ma, J. M. Mabry, S. A. Mazzella, G. C. Rutledge, G. H. McKinley, R. E. Cohen, *Science* **2007**, *318*, 5856.
[6] E. P. Chan, E. J. Smith, R. C. Hayward, A. J. Crosby, *Adv. Mater.* **2008**, *20*, 4.
[7] T. K. Bhandakkar, H. T. Johnson, *J. Mech. Phys. Solids* **2012**, *60*, 6.
[8] L. M. Mathger, E. J. Denton, N. J. Marshall, R. T. Hanlon, *J. R. Soc. Interface* **2009**, *6*, 105.
[9] K. Efimenko, M. Rackaitis, E. Manias, A. Vaziri, L. Mahadevan, J. Genzer, *Nat. Mater.* **2005**, *4*, 4.
[10] N. Bowden, S. Brittain, A. G. Evans, J. W. Hutchinson, G. M. Whitesides, *Nature* **1998**, *393*, 6681.
[11] E. Cerda, L. Mahadevan, *Phys. Rev. Lett.* **2003**, *90*, 7.
[12] S. Cai, D. Breid, A. J. Crosby, Z. Suo, J. W. Hutchinson, *J. Mech. Phys. Solids* **2011**, *59*, 5.
[13] A. N. Gent, I. S. Cho, *Rubber Chem. Technol.* **1999**, *72*, 2.
[14] W. Hong, X. Zhao, Z. Suo, *Appl. Phys. Lett.* **2009**, *95*, 11.
[15] L. Zhai, M. C. Berg, F. C. Cebeci, Y. Kim, J. M. Milwid, M. F. Rubner, R. E. Cohen, *Nano Lett.* **2006**, *6*, 6.